# Spectral Image Fusion from Compressive Projections Using Total-Variation and Low-Rank Regularizations

Tatiana Gelvez
*Department of Electrical Engineering*
*Universidad Industrial de Santander*
*Bucaramanga, Colombia 680002*
*Email: tatiana.gelvez@correo.uis.edu.co*

Henry Arguello
*Department of Computer Science*
*Universidad Industrial de Santander*
*Bucaramanga, Colombia 680002*
*Email: henarfu@uis.edu.co*

*Abstract*—**This work presents a spectral image fusion approach from compressive projections based on the linear mixture model that exploits the endmember matrix low dimensional structure. The formulated inverse problem includes a total variation term over the abundance matrix to promote smoothness, but also a low rank term over the endmember matrix to promote the low rank structure. The optimization problem is solved using an alternating direction method of multipliers (ADMM) approach to independently estimate the abundance and endmember matrices. Simulations show that the fusion problem can be effectively solved from compressive projections, and the inclusion of the low rank regularization increases the reconstruction quality.**

## 1. Introduction

Spectral images contain a portion of the electromagnetic spectrum along many narrow spectral bands. This information allows to better identify objects based on their reflectance spectra and to find detailed object properties [1]. Common spectral imaging sensors are able to capture either a high spatial resolution, known as multispectral images (MS), or a high spectral resolution, known as hyperspectral images (HS), but not both at the same time [2]. Then, a fusion methods can be used to obtain a high spatio-spectral resolution scene by fusing the MS and HS images [3]. Recently, the compressive spectral imaging (CSI) framework has allowed to reduce the number of sampled pixels by encoding and dispersing the spectral information along the spatial domain of a scene [4]. Hence, this work proposes to solve the fusion inverse problem to obtain a high resolution scene from compressed projections of the MS and HS images. The proposed formulation is based on the linear mixture model of the spectral scene, similiar to the approach presented in [2], with the difference that we use compressed measurements instead of the full MS and HS images. Further, we aim at estimating both, the abundance and the endmember matrices. To do that, the proposed inverse problem includes traditional specific characteristics on the abundance matrix, as the smoothness promoted by a total variation (TV) regularizer, but also as a new contribution, it promotes a low rank structure on the endmember matrix, which is regularized with a nuclear norm term. The inverse spectral fusion problem formulation results in minimizing an objective function which includes two fidelity data terms, a TV regularization, and a low-rank penalty. In order to independently estimate the endmember and abundance matrices, we employ an alternating ADMM approach. Simulations over two well-known databases were carried out to measure the performance of the proposed method in terms of the normalized mean squared error, the spectral angle mapper, and the peak signal to noise ratio metrics. Results show that the high spatio-spectral resolution scene can be properly estimated from compressed projections using the proposed regularizations.

## 2. Compressive Fusion Observation Model

Let $\mathbf{Z} \in \mathbb{R}^{L_h \times n_m}$ denote a high spatio-spectral resolution (HR) scene with $L_h$ spectral bands and $n_m$ spatial pixels. Then, the observation model of the compressive fusion problem can be written

$$\mathbf{Y}_h = \mathbf{H}_h\mathbf{Z}\mathbf{B}\mathbf{M} + \mathbf{N}_h, \tag{1}$$

$$\mathbf{Y}_m = \mathbf{H}_m\mathbf{R}\mathbf{Z} + \mathbf{N}_m. \tag{2}$$

In (1) the matrix $\mathbf{B} \in \mathbb{R}^{n_m \times n_m}$ is a spatial convolution operator, $\mathbf{M} \in \mathbb{R}^{n_m \times n_h}$ represents a uniform subsampling operator, and so, the HS scene $\mathbf{Z}^{HS} \in \mathbb{R}^{L_h \times n_h} = \mathbf{ZBM}$ is assumed to be a blurred and downsampled version of the target $\mathbf{Z}$ by a factor of $d_h$, such that, the number of spatial pixels corresponds to $n_h = n_m/d_h^2$; $\mathbf{H}_h \in \mathbb{R}^{m_h \times L_h}$ denotes the sensing matrix with $m_h \ll L_h$ used to obtain the HS compressed measurements $\mathbf{Y}_h \in \mathbb{R}^{m_h \times n_h}$, and $\mathbf{N}_h \in \mathbb{R}^{m_h \times n_h}$ is a Gaussian noise matrix. Similarly, in (2) $\mathbf{R} \in \mathbb{R}^{L_m \times L_h}$ contains the spectral response of the sensor, and so, the MS scene $\mathbf{Z}^{MS} \in \mathbb{R}^{L_m \times n_m} = \mathbf{RZ}$ is assumed to be a spectrally degraded version of the target $\mathbf{Z}$ by a factor of $d_m$, such that, the number of spectral bands are $L_m = L_h/d_m$; $\mathbf{H}_m \in \mathbb{R}^{m_m \times L_m}$ denotes the sensing matrix with $m_m \ll L_m$ used to obtain the MS compressed measurements $\mathbf{Y}_m \in \mathbb{R}^{m_m \times n_m}$, and $\mathbf{N}_m \in \mathbb{R}^{m_m \times n_m}$ is a Gaussian noise matrix.

ISBN 978-90-827970-1-5 

Because spectral images exhibit high spectral correlations, it is assumed that the HR scene lies in a low dimensional subspace [5]. Hence, it can be written as the product of two matrices, $\mathbf{Z} = \mathbf{EX}$, known as the linear mixture model [6], where $\mathbf{E} \in \mathbb{R}^{L_h \times k}$ is named the endmember matrix containing $k \ll L_h$ endmembers that span the matrix $\mathbf{Z}$, and $\mathbf{X} \in \mathbb{R}^{k \times n_m}$ is named the abundance matrix which contains the proportion of each endmember present at each spatial pixel [7]. Thus, the observation model using the linear mixture becomes,

$$\mathbf{Y}_h = \mathbf{H}_h\mathbf{EXBM} + \mathbf{N}_h, \tag{3}$$

$$\mathbf{Y}_m = \mathbf{H}_m\mathbf{REX} + \mathbf{N}_m. \tag{4}$$

Note, in Eqs. (3) and (4) that the full HR scene is replaced by the product of the endmember and abundance matrices.

## 3. Compressive Fusion Inverse Problem Formulation

This section introduces an optimization problem to estimate the endmember and abundance matrices from the compressed measurements in Eqs. (3) and (4) instead of recovering the high resolution scene. To do that, we seek to minimize an objective function which includes two fidelity data terms corresponding to the compressed MS and HS observations, respectively. Specifically, the matrices $\mathbf{E}$ and $\mathbf{X}$ can be estimated as

$$\begin{aligned}\hat{\mathbf{E}}, \hat{\mathbf{X}} = \underset{\mathbf{E},\mathbf{X}}{\text{argmin}}\ & \frac{1}{2}\|\mathbf{H}_h\mathbf{EXBM} - \mathbf{Y}_h\|_F^2 + \\ & \frac{\lambda}{2}\|\mathbf{H}_m\mathbf{REX} - \mathbf{Y}_m\|_F^2\end{aligned} \tag{5}$$

where $\lambda > 0$ is a parameter to control the relative weight of the term. Since the inverse problem in (5) is ill-posed [8], further regularizers and constraints over the abundance and endmember matrices are required. Traditional regularizations over the abundance matrix include:

- A Total Variation (TV) regularizer to promote smooth transitions, $\tau\phi_1(\mathbf{X}) = \tau\|\mathbf{XD}_v\|_1 + \tau\|\mathbf{XD}_h\|_1$, where $\mathbf{D}_v \in \mathbb{R}^{n_m \times n_m}$, and $\mathbf{D}_h \in \mathbb{R}^{n_m \times n_m}$ correspond to the vertical and horizontal discrete difference operators, respectively, with $\tau > 0$ [9], and the $\ell_1$-norm is defined as the sum of the absolute values of the matrix. Thus, for a matrix $\mathbf{O} \in \mathbb{R}^{n \times n}$, $\|\mathbf{O}\|_1 = \sum_{i=1}^{n}\sum_{j=1}^{n}|O_{i,j}|$. Different regularizations for hyperspectral images as the structure tensor regularization in [10] could be also used.
- A non-negativity constraint to indicate that the fractional abundances can not be negative, modeled as $\mathbf{X} \geq 0$ [11].
- A sum-to-one constraint to consider the entire composition of a mixed pixel, modeled as $\mathbf{1}_k^T\mathbf{X} = \mathbf{1}_{n_m}^T$ [12].

On the other hand, traditional constraints over the endmember matrix impose that each spectral signature represents the reflectances of different materials that belong to the interval $[0, 1]$. Thus, $\mathbf{E} \in [0, 1]^{L_h \times k}$ [11], [13].

The contribution of this work is the imposition of an additional regularization over the endmember matrix to promote a low rank structure. This comes from the assumption that the high resolution scene is low rank since there exist few different endmembers which are enough to represent the complete data [6]. Then, we aim at minimizing the rank of the endmember matrix by using the traditional nuclear norm relaxation as $\gamma\|\mathbf{E}\|_*$, with $\gamma > 0$ [14]. Including the TV and low-rank regularizations together with the non-negativity, the sum-to-one, and the reflectance constraints, the compressive fusion inverse problem based on the linear mixture model in (5) can be rewritten as

$$\begin{aligned}\hat{\mathbf{E}}, \hat{\mathbf{X}} = \underset{\mathbf{E},\mathbf{X}}{\text{argmin}} & \frac{1}{2}\|\mathbf{H}_h\mathbf{EXBM} - \mathbf{Y}_h\|_F^2 + \\ & \frac{\lambda}{2}\|\mathbf{H}_m\mathbf{REX} - \mathbf{Y}_m\|_F^2 + \\ & \tau\|\mathbf{XD}_v\|_1 + \tau\|\mathbf{XD}_h\|_1 + \gamma\|\mathbf{E}\|_* \\ \text{subject to} \quad & \mathbf{X} \geq 0; \quad \mathbf{1}_k^T\mathbf{X} = \mathbf{1}_{n_m}^T; \quad 0 \leq \mathbf{E} \leq 1.\end{aligned} \tag{6}$$

## 4. TV and Low-Rank based Compressive Fusion Numerical Algorithm

The problem in (6) is nonconvex since it presents a quadratic formulation over variables $\mathbf{E}$ and $\mathbf{X}$. To solve this nonconvex inverse problem we follow a block coordinate descent method [15], [16] which allows to alternate the optimization variables in order to solve independently for each of them, assuming that the other variable is fixed. Each independent solving algorithm follows an ADMM approach. The general scheme of the proposed numerical algorithm is summarized in Algorithm 1. Details about the optimization subproblems are presented in the subsections bellow.

**Algorithm 1** Compressive image fusion using TV and Low Rank Regularizations

**procedure** CIF($\mathbf{H}_h, \mathbf{H}_m, \mathbf{M}, \mathbf{R}, \mathbf{Y}_h, \mathbf{Y}_m, , \mathbf{B}, \mathbf{D}_v, \mathbf{D}_h$, Iter)
    $w \leftarrow 0$
    $\mathbf{E}^w \sim U[0, 1]$ ▷ Random initialization
    **while** $w <$ Iter **do**
        $\mathbf{X}^{w+1} \leftarrow$ Solve (6) with $\mathbf{E}$ fixed. ▷ Algorithm 2
        $\mathbf{E}^{w+1} \leftarrow$ Solve (6) with $\mathbf{X}$ fixed. ▷ Algorithm 3
        $w \leftarrow w + 1$
    **end while**
    **return** $\mathbf{X}^{\text{Iter}}$ and $\mathbf{E}^{\text{Iter}}$
**end procedure**

### 4.1. Abundance Matrix Estimation using ADMM

Assuming that the endmember matrix ($\mathbf{E}$) is fixed, the inverse problem to estimate the abundance matrix ($\mathbf{X}$) corresponds to,

$$\begin{aligned}\hat{\mathbf{X}} = \underset{\mathbf{X} \in \mathbb{R}^{k \times n_m}}{\text{argmin}} & \|\mathbf{H}_h\mathbf{EXBM} - \mathbf{Y}_h\|_F^2 + \\ & \lambda\|\mathbf{H}_m\mathbf{REX} - \mathbf{Y}_m\|_F^2 + \\ & 2\tau\|\mathbf{XD}_v\|_1 + 2\tau\|\mathbf{XD}_h\|_1 + \phi_2(\mathbf{X}),\end{aligned} \tag{7}$$

ISBN 978-90-827970-1-5 © EURASIP 2018

where $\phi_2(\cdot)$ is an indicator function that accounts for the sum-to-one constraint

$$\phi_2(\mathbf{X}) = \begin{cases} 0, & \mathbf{X} \in \mathcal{P} \\ \infty, & \mathbf{X} \notin \mathcal{P} \end{cases}, \tag{8}$$

with $\mathcal{P} = \{\mathbf{P} | \mathbf{P} \geq 0, \mathbf{1}_k^T \mathbf{P} = \mathbf{1}_{n_m}^T\}$. Observe that, the non-negative and sum-to-one constraints in (6) were replaced by this indicator function which implies that the cost function can take values in the extended real number line $\widetilde{\mathbb{R}} = \mathbb{R} \cup \{\infty\}$.

The first step to solve problem in (7) is to include the auxiliary splitting variables which yields to,

$$\begin{aligned} \hat{\mathbf{X}}, \hat{\mathbf{V}}_i = & \underset{\mathbf{X}, \mathbf{V}_i}{\operatorname{argmin}} \quad \|\mathbf{H}_h \mathbf{E} \mathbf{V}_1 \mathbf{M} - \mathbf{Y}_h\|_F^2 + \\ & \lambda \|\mathbf{H}_m \mathbf{R} \mathbf{E} \mathbf{V}_2 - \mathbf{Y}_m\|_F^2 + \\ & 2\tau \|\mathbf{V}_3\|_1 + 2\tau \|\mathbf{V}_4\|_1 + \phi_2(\mathbf{V}_5), \\ \text{subject to} \quad & \mathbf{X}\mathbf{B} = \mathbf{V}_1; \;\; \mathbf{X} = \mathbf{V}_2; \;\; \mathbf{X}\mathbf{D}_v = \mathbf{V}_3; \\ & \mathbf{X}\mathbf{D}_h = \mathbf{V}_4; \;\; \mathbf{X} = \mathbf{V}_5. \end{aligned} \tag{9}$$

The augmented Lagrangian associated with (9) corresponds to

$$\begin{aligned} \mathcal{L}(\hat{\mathbf{X}}, \hat{\mathbf{V}}_i, \hat{\mathbf{D}}_i) = & \underset{\mathbf{X}, \mathbf{V_i}, \mathbf{D}_i}{\operatorname{argmin}} \; \|\mathbf{H}_h \mathbf{E} \mathbf{V}_1 \mathbf{M} - \mathbf{Y}_h\|_F^2 + \\ & \lambda \|\mathbf{H}_m \mathbf{R} \mathbf{E} \mathbf{V}_2 - \mathbf{Y}_m\|_F^2 + \\ & \rho \|\mathbf{X}\mathbf{B} - \mathbf{V}_1 - \mathbf{D}_1\|_F^2 + \\ & \rho \|\mathbf{X} - \mathbf{V}_2 - \mathbf{D}_2\|_F^2 + \\ & 2\tau \|\mathbf{V}_3\|_1 + \rho \|\mathbf{X}\mathbf{D}_v - \mathbf{V}_3 - \mathbf{D}_3\|_F^2 + \\ & 2\tau \|\mathbf{V}_4\|_1 + \rho \|\mathbf{X}\mathbf{D}_h - \mathbf{V}_4 - \mathbf{D}_4\|_F^2 + \\ & \phi_2(\mathbf{V}_5) + \rho \|\mathbf{X} - \mathbf{V}_5 - \mathbf{D}_5\|_F^2, \end{aligned} \tag{10}$$

with $\rho > 0$. Minimization over each variable $\mathbf{X}, \mathbf{V}_i$, and $\mathbf{D}_i$ in (10) leads to the closed solutions summarized in Algorithm 2 from line 6 to line 16. In line 7, $\circ$ denotes the Hadamard product, and $\widetilde{\mathbf{M}}$ is an equivalent matrix to the subsampling matrix $\mathbf{M}$. In line 9 and line 10 soft.$(\cdot)$ indicates the soft thresholding operator such that for a structure $\mathbf{o} \in \mathbb{R}^n$,

$$\operatorname{soft}_\xi(\mathbf{o}) = \begin{cases} 0, & o_i \leq \xi \\ o_i, & o_i > \xi \end{cases} \quad \text{for } i = 1 \ldots n. \tag{11}$$

In line 11 SimplexProjection$(\cdot)$ indicates the Euclidean projection on $\mathcal{P}$.

### 4.2. Endmember Matrix Estimation using ADMM

The minimization problem to estimate the endmember matrix $\mathbf{E}$ for a fixed $\mathbf{X}$ corresponds to,

$$\begin{aligned} \hat{\mathbf{E}} = & \underset{\mathbf{E}}{\operatorname{argmin}} \; \|\mathbf{H}_h \mathbf{E} \mathbf{X} \mathbf{B} \mathbf{M} - \mathbf{Y}_h\|_F^2 + \\ & \lambda \|\mathbf{H}_m \mathbf{R} \mathbf{E} \mathbf{X} - \mathbf{Y}_m\|_F^2 + 2\gamma \|\mathbf{E}\|_* + \psi_1(\mathbf{E}), \end{aligned} \tag{12}$$

where $\psi_1(\cdot)$ is an indicator function that accounts for the reflectance constraint

$$\psi_1(\mathbf{E}) = \begin{cases} 0, & \mathbf{E} \in \mathcal{Q} \\ \infty, & \mathbf{E} \notin \mathcal{Q} \end{cases}; \; \mathcal{Q} = \{\mathbf{Q} | 0 \leq \mathbf{Q} \leq 1\}. \tag{13}$$

**Algorithm 2** Abundance Estimation with ADMM approach

1: **procedure** AbundanceADMM($\mathbf{H}_h, \mathbf{H}_m, \mathbf{M}, \mathbf{R}, \mathbf{Y}_h, \mathbf{Y}_m, , \mathbf{B}, \mathbf{D}_v, \mathbf{D}_h, \mathbf{E}^w, \lambda, \tau, \rho$, IterX)
2: $\quad u \leftarrow 0$
3: $\quad \mathbf{V}_i^u \leftarrow \mathbf{0}$
4: $\quad \mathbf{D}_i^u \leftarrow \mathbf{0}$
5: $\quad$ **while** $u <$ IterX **do**
6: $\quad\quad \mathbf{X}^{u+1} \leftarrow [(\mathbf{V}_1^u + \mathbf{D}_1^u)\mathbf{B}^T + (\mathbf{V}_2^u + \mathbf{D}_2^u) + (\mathbf{V}_3^u + \mathbf{D}_3^u)\mathbf{D}_v^T + (\mathbf{V}_4^u + \mathbf{D}_4^u)\mathbf{D}_h^T + (\mathbf{V}_5^u + \mathbf{D}_5^u)][\mathbf{B}\mathbf{B}^T + \mathbf{D}_v\mathbf{D}_v^T + \mathbf{D}_h\mathbf{D}_h^T + 2\mathbf{I}]^{-1}$
7: $\quad\quad \mathbf{V}_1^{u+1} \leftarrow [(\mathbf{H}_h\mathbf{E}^w)^T(\mathbf{H}_h\mathbf{E}^w) + \rho\mathbf{I}]^{-1} [(\mathbf{H}_h\mathbf{E}^w)^T\mathbf{Y}_h\mathbf{M}^T + \rho(\mathbf{X}^{u+1}\mathbf{B} - \mathbf{D}_1^u)] \circ \widetilde{\mathbf{M}} + [(\mathbf{X}^{u+1}\mathbf{B} - \mathbf{D}_1^u) \circ (\mathbf{1} - \widetilde{\mathbf{M}})]$
8: $\quad\quad \mathbf{V}_2^{u+1} \leftarrow [\lambda(\mathbf{H}_m\mathbf{R}\mathbf{E}^w)^T(\mathbf{H}_m\mathbf{R}\mathbf{E}^w) + \rho\mathbf{I}]^{-1} [\lambda(\mathbf{H}_m\mathbf{R}\mathbf{E}^w)^T\mathbf{Y}_m + \rho(\mathbf{X}^{u+1} - \mathbf{D}_2^u)]$
9: $\quad\quad \mathbf{V}_3^{u+1} \leftarrow \operatorname{soft}_{2\tau/\rho}(\mathbf{X}^{u+1}\mathbf{D}_v - \mathbf{D}_3^u)$
10: $\quad\quad \mathbf{V}_4^{u+1} \leftarrow \operatorname{soft}_{2\tau/\rho}(\mathbf{X}^{u+1}\mathbf{D}_h - \mathbf{D}_4^u)$
11: $\quad\quad \mathbf{V}_5^{u+1} \leftarrow \operatorname{SimplexProjection}(\mathbf{X}^{u+1} - \mathbf{D}_5^u)$
12: $\quad\quad \mathbf{D}_1^{u+1} \leftarrow \mathbf{D}_1^u + \mathbf{V}_1^{u+1} - \mathbf{X}^{u+1}\mathbf{B}$
13: $\quad\quad \mathbf{D}_2^{u+1} \leftarrow \mathbf{D}_2^u + \mathbf{V}_2^{u+1} - \mathbf{X}^{u+1}$
14: $\quad\quad \mathbf{D}_3^{u+1} \leftarrow \mathbf{D}_3^u + \mathbf{V}_3^{u+1} - \mathbf{X}^{u+1}\mathbf{D}_v$
15: $\quad\quad \mathbf{D}_4^{u+1} \leftarrow \mathbf{D}_4^u + \mathbf{V}_4^{u+1} - \mathbf{X}^{u+1}\mathbf{D}_h$
16: $\quad\quad \mathbf{D}_5^{u+1} \leftarrow \mathbf{D}_5^u + \mathbf{V}_5^{u+1} - \mathbf{X}^{u+1}$
17: $\quad\quad u \leftarrow u + 1$
18: $\quad$ **end while**
19: $\quad$ **return** $\mathbf{X}^{\text{IterX}}$
20: **end procedure**

The first step to solve problem in (12) is to include the auxiliary splitting variables which yields to,

$$\begin{aligned} \hat{\mathbf{E}}, \hat{\mathbf{W}}_j = & \underset{\mathbf{E}, \mathbf{W}_j}{\operatorname{argmin}} \quad \|\mathbf{W}_1 \mathbf{X} \mathbf{B} \mathbf{M} - \mathbf{Y}_h\|_F^2 + \\ & \lambda \|\mathbf{W}_2 \mathbf{X} - \mathbf{Y}_m\|_F^2 + \\ & 2\gamma \|\mathbf{W}_3\|_* + \psi_1(\mathbf{W}_4), \\ \text{subject to} \quad & \mathbf{H}_h \mathbf{E} = \mathbf{W}_1; \;\; \mathbf{H}_m \mathbf{R} \mathbf{E} = \mathbf{W}_2; \\ & \mathbf{E} = \mathbf{W}_3; \;\; \mathbf{E} = \mathbf{W}_4. \end{aligned} \tag{14}$$

Then, the augmented Lagrangian associated with (14) corresponds to

$$\begin{aligned} \mathcal{L}(\hat{\mathbf{E}}, \hat{\mathbf{W}}_j, \hat{\mathbf{G}}_j) = & \underset{\mathbf{E}, \mathbf{W}_j, \mathbf{G}_j}{\operatorname{argmin}} \; \|\mathbf{W}_1 \mathbf{X} \mathbf{B} \mathbf{M} - \mathbf{Y}_h\|_F^2 + \\ & \lambda \|\mathbf{W}_2 \mathbf{X} - \mathbf{Y}_m\|_F^2 + 2\gamma \|\mathbf{W}_3\|_* + \\ & \psi_1(\mathbf{W}_4) + \chi \|\mathbf{H}_h \mathbf{E} - \mathbf{W}_1 - \mathbf{G}_1\|_F^2 + \\ & \chi \|\mathbf{H}_m \mathbf{R} \mathbf{E} - \mathbf{W}_2 - \mathbf{G}_2\|_F^2 + \\ & \chi \|\mathbf{E} - \mathbf{W}_3 - \mathbf{G}_3\|_F^2 + \\ & \chi \|\mathbf{E} - \mathbf{W}_4 - \mathbf{G}_4\|_F^2, \end{aligned} \tag{15}$$

with $\chi > 0$. Minimization over each variable $\mathbf{E}, \mathbf{W}_j$, and $\mathbf{G}_j$ in (15) leads to the closed solutions summarized in Algorithm 3 from line 6 to line 15. There, in line 9 $\mathbf{U}$ and $\mathbf{V}$ are the left and right eigenvectors associated with the eigenvalues in $\boldsymbol{\sigma}$, and in line 11 the min max operator approximates the projection onto $\mathcal{Q}$.

ISBN 978-90-827970-1-5 © EURASIP 2018

**Algorithm 3** Endmember Estimation with ADMM approach

**procedure** ENDMEMBER-ADMM($\mathbf{H}_h, \mathbf{H}_m, \mathbf{M}, \mathbf{R}, \mathbf{Y}_h, \mathbf{Y}_m, , \mathbf{B}, \mathbf{X}^{w+1}, \lambda, \gamma, \chi$, IterE)

  $v \leftarrow 0$

  $\mathbf{W}_j^v \leftarrow \mathbf{0}$

  $\mathbf{G}_j^v \leftarrow \mathbf{0}$

  **while** $v <$ IterE **do**

    $\mathbf{E}^{v+1} \leftarrow [\mathbf{H}_h^T\mathbf{H}_h + (\mathbf{H}_m\mathbf{R})^T(\mathbf{H}_m\mathbf{R}) + 2\mathbf{I}]^{-1} [\mathbf{H}_h^T(\mathbf{W}_1^v+\mathbf{G}_1^v) + (\mathbf{H}_m\mathbf{R})^T(\mathbf{W}_2^v+\mathbf{G}_2^v) + (\mathbf{W}_3^v+\mathbf{G}_3^v) + (\mathbf{W}_4^v+\mathbf{G}_4^v)]$

    $\mathbf{W}_1^{v+1} \leftarrow [\mathbf{Y}_h(\mathbf{X}^{w+1}\mathbf{B}\mathbf{M})^T + \chi(\mathbf{H}_h\mathbf{E}^{v+1} - \mathbf{G}_1^v)]\ [(\mathbf{X}^{w+1}\mathbf{B}\mathbf{M})(\mathbf{X}^{w+1}\mathbf{B}\mathbf{M})^T + \chi\mathbf{I}]^{-1}$

    $\mathbf{W}_2^{v+1} \leftarrow [\lambda(\mathbf{Y}_m(\mathbf{X}^{w+1})^T + \chi(\mathbf{H}_m\mathbf{R}\mathbf{E}^{v+1} - \mathbf{G}_2^v)][\lambda(\mathbf{X}^{w+1})(\mathbf{X}^{w+1})^T + \chi\mathbf{I}]^{-1}$

    $[\mathbf{U}, \boldsymbol{\sigma}, \mathbf{V}] \leftarrow \text{svd}(\mathbf{E}^{v+1} - \mathbf{G_3}^v)$ ▷ Singular Value Decomposition

    $\mathbf{W}_3^{v+1} \leftarrow \mathbf{U}(\text{soft}_{2\gamma/\chi}(\boldsymbol{\sigma})\mathbf{V}^T$

    $\mathbf{W}_4^{v+1} \leftarrow \min(\max(0, \mathbf{E} - \mathbf{G_4}), 1)$

    $\mathbf{G}_1^{v+1} \leftarrow \mathbf{G}_1^v + \mathbf{W}_1^{v+1} - \mathbf{H}_h\mathbf{E}^{v+1}$

    $\mathbf{G}_2^{v+1} \leftarrow \mathbf{G}_2^v + \mathbf{W}_2^{v+1} - \mathbf{H}_m\mathbf{R}\mathbf{E}^{v+1}$

    $\mathbf{G}_3^{v+1} \leftarrow \mathbf{G}_3^v + \mathbf{W}_3^{v+1} - \mathbf{E}^{v+1}$

    $\mathbf{G}_4^{v+1} \leftarrow \mathbf{G}_4^v + \mathbf{W}_4^{v+1} - \mathbf{E}^{v+1}$

    $v \leftarrow v + 1$

  **end while**

  **return** $\mathbf{E}^{\text{IterE}}$

**end procedure**

## 5. Results

The evaluation of the proposed compressive fusion using TV and low rank regularizations was realized using:

- the Jasper database **F1** taken from [17] with $L_h = 198$ spectral bands, $n_m = 10000$ spatial pixels, and $k = 4$ endmembers.
- a section of the Urban database **F2** taken from [17] with $L_h = 162$ spectral bands, $n_m = 16384$ spatial pixels, $k = 6$ endmembers.

In both cases, the HS scene is a blur downsampled version by a factor $d_h = 4$ and the MS scene is a spectrally degraded version by a factor $d_m = 2$. The entries of the matrices $\mathbf{H}_h$ and $\mathbf{H}_m$ were generated using a Bernoulli distribution modelling different optical filters. For **F1** there were acquired $m_h = 66$ shots of the HS scene, and $m_m = 33$ shots of the MS scene; for **F2** there were acquired $m_h = 54$ shots of the HS scene, and $n_m = 27$ shots of the MS scene which represent the 33% of the data, approximately. We use the peak signal to noise ratio (PSNR) to measure the visual quality of the reconstructions, the normalized mean square error (NMSE), and the spectral angle mapper (SAM) metrics to measure the quality of the unmixing results. The results are compared to the approach presented in [18] that estimates the endmember and abundance matrices just using the TV regularization.

Figure 1 shows the original and the visualization of the endmembers and the fractional abundances for both databases. Tables 1 and 2 show the average of the PSNR, SAM, NMSE$_E$ (for endmembers), NMSE$_X$ (for abundances) metrics in noisy scenarios with 10, 20, 30, and 40 [dB] of SNR to compare the proposed joint TV and Low Rank compressive fusion approach denoted as TL, with respect to the compressive TV approach for the **F1** and **F2** databases, respectively. Note that the proposed approach exhibits a better estimation quality performance in exchange of a higher running time.

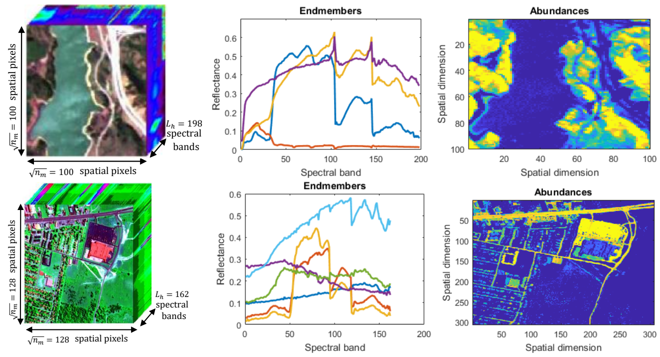


Figure 1. *Top:* Jasper **F1** high spatio-spectral resolution scene with $k = 4$ known endmembers and their abundances. *Bottom:* Urban **F2** high spatio-spectral resolution scene with $k = 6$ known endmembers and their abundances.

TABLE 1. METRICS COMPARISON BETWEEN THE COMPRESSIVE TV AND THE JOINT TV-LOW RANK COMPRESSIVE APPROACHES **F1**

| Metric \ SNR Noise | | 10 [dB] | 20 [dB] | 30 [dB] | 40 [dB] |
|---|---|---|---|---|---|
| **Spatial PSNR** | TV | 12.9699 | 14.8010 | 17.0252 | 26.0860 |
| | TL | **17.4053** | **23.9369** | **27.8520** | **28.8599** |
| **Spectral PSNR** | TV | 10.8878 | 13.1913 | 15.5043 | 25.1604 |
| | TL | **18.2326** | **24.4099** | **26.9205** | **27.4579** |
| **SAM** | TV | 34.1871 | 27.8023 | 20.3515 | 9.6297 |
| | TL | **18.8465** | **8.5610** | **5.0913** | **4.7947** |
| **NMSE$_E$** | TV | 2.7956 | 1.9883 | **−5.6778** | **−3.1860** |
| | TL | **−0.8339** | **−1.1881** | −2.3914 | −2.4666 |
| **NMSE$_X$** | TV | −1.6784 | 1.8091 | 0.2546 | 3.6186 |
| | TL | **−2.2642** | **−3.5914** | **−1.8835** | **−2.5434** |
| **Time [s]** | TV | **6.6907** | **6.6542** | **6.6175** | **6.6161** |
| | TL | 36.6490 | 35.8204 | 35.1335 | 35.0655 |

TABLE 2. METRICS COMPARISON BETWEEN THE COMPRESSIVE TV AND THE JOINT TV-LOW RANK COMPRESSIVE APPROACHES **F2**

| Metric \ SNR Noise | | 10 [dB] | 20 [dB] | 30 [dB] | 40 [dB] |
|---|---|---|---|---|---|
| **Spatial PSNR** | TV | 14.0104 | 16.7830 | 20.2627 | 24.9318 |
| | TL | **16.4159** | **22.3619** | **31.4102** | **35.7441** |
| **Spectral PSNR** | TV | 12.6185 | 16.6203 | 18.8364 | 21.0864 |
| | TL | **15.1395** | **20.4813** | **26.5066** | **28.3037** |
| **SAM** | TV | 35.0039 | 27.7122 | 16.7771 | 9.5743 |
| | TL | **24.3231** | **10.2250** | **4.5018** | **3.8296** |
| **NMSE$_E$** | TV | 7.3850 | **0.7769** | **−5.7855** | **−6.0292** |
| | TL | **7.0381** | 2.6618 | 1.4712 | −1.8018 |
| **NMSE$_X$** | TV | 1.6914 | 4.1353 | 3.5939 | 4.9131 |
| | TL | **−0.0246** | **0.8392** | **−0.3481** | **−0.2788** |
| **Time [s]** | TV | **15.1232** | **14.8689** | **14.7896** | **14.8538** |
| | TL | 118.3716 | 90.6913 | 124.1256 | 122.6113 |

ISBN 978-90-827970-1-5  

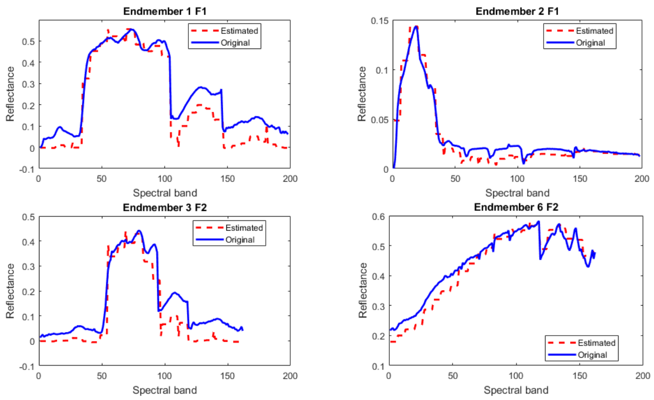


Figure 2. Visual comparison of some estimated endmembers for databases *Top:* $\mathbf{F1}$ and *Bottom:* $\mathbf{F2}$.

Figure 2 shows a visual comparison of the original endmembers with respect to the estimated using the compressive joint TV and Low Rank approach for the databases $\mathbf{F1}$ and $\mathbf{F2}$ in a scenario of $40$ [db] of noise. Finally, Fig. 3 shows the estimated fractional abundances associated with the estimated endmembers showed in Fig. 2.

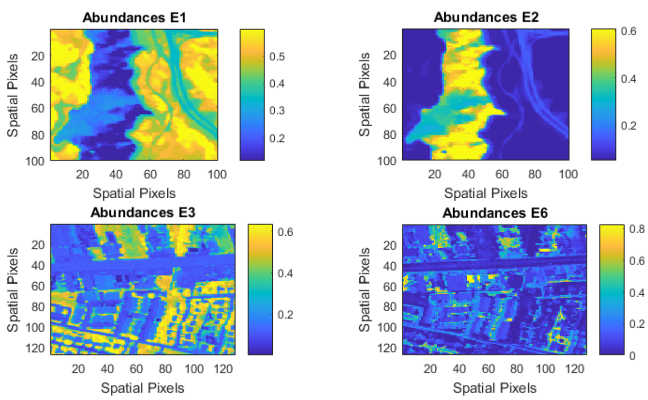


Figure 3. Visual comparison of the estimated fractional abundances for databases *Top:* $\mathbf{F1}$ and *Bottom:* $\mathbf{F2}$.

## 6. Conclusion

This work presented an approach to solve the fusion problem from compressive projections. The proposed method is based on the well known linear mixture model in order to estimate the endmember and abundance matrices instead of the complete image. The inverse problem formulation includes the traditional total variation, nonnegative, and sum-to-one terms. Further, as a contribution the minimization of the nuclear norm of the endmember matrix is included in order to promote a low rank structure. The resulting nonconvex problem was solved under the block coordinate descent method in which the estimation of the endmember and abundance matrices were realized independently under an ADMM approach. Simulations and results show that the fusion problem can be effectively solved by using compressive projections exploiting the linear mixture model and a low rank regularization.

## References


[1] H. Rueda, H. Arguello, and G. R. Arce, "Dmd-based implementation of patterned optical filter arrays for compressive spectral imaging," *JOSA A*, vol. 32, no. 1, pp. 80–89, 2015.

[2] A. Teodoro, J. Bioucas-Dias, and M. Figueiredo, "Sharpening hyperspectral images using plug-and-play priors," pp. 392–402, Springer International Publishing, 2017.

[3] Z. Chen, H. Pu, B. Wang, and G. M. Jiang, "Fusion of hyperspectral and multispectral images: A novel framework based on generalization of pan-sharpening methods," *IEEE Geoscience and Remote Sensing Letters*, vol. 11, pp. 1418–1422, Aug 2014.

[4] C. V. Correa, H. Arguello, and G. R. Arce, "Spatiotemporal blue noise coded aperture design for multi-shot compressive spectral imaging," *JOSA A*, vol. 33, no. 12, pp. 2312–2322, 2016.

[5] G. Martn and J. M. Bioucas-Dias, "Spatial-spectral hyperspectral image compressive sensing," in *2017 IEEE International Geoscience and Remote Sensing Symposium (IGARSS)*, pp. 3988–3991, July 2017.

[6] J. M. Bioucas-Dias, A. Plaza, N. Dobigeon, M. Parente, Q. Du, P. Gader, and J. Chanussot, "Hyperspectral unmixing overview: Geometrical, statistical, and sparse regression-based approaches," *IEEE journal of selected topics in applied earth observations and remote sensing*, vol. 5, no. 2, pp. 354–379, 2012.

[7] Q. Wei, J. M. Bioucas-Dias, N. Dobigeon, and J.-Y. Tourneret, "Fusion of multispectral and hyperspectral images based on sparse representation," in *Signal Processing Conference (EUSIPCO), 2014 Proceedings of the 22nd European*, pp. 1577–1581, IEEE, 2014.

[8] J. Yang, J. Wright, T. S. Huang, and Y. Ma, "Image super-resolution via sparse representation," *IEEE transactions on image processing*, vol. 19, no. 11, pp. 2861–2873, 2010.

[9] M.-D. Iordache, J. M. Bioucas-Dias, and A. Plaza, "Total variation spatial regularization for sparse hyperspectral unmixing," *IEEE Transactions on Geoscience and Remote Sensing*, vol. 50, no. 11, pp. 4484–4502, 2012.

[10] G. Chierchia, N. Pustelnik, B. Pesquet-Popescu, and J.-C. Pesquet, "A nonlocal structure tensor-based approach for multicomponent image recovery problems," *IEEE Transactions on Image Processing*, vol. 23, no. 12, pp. 5531–5544, 2014.

[11] S. Jia and Y. Qian, "Constrained nonnegative matrix factorization for hyperspectral unmixing," *IEEE Transactions on Geoscience and Remote Sensing*, vol. 47, no. 1, pp. 161–173, 2009.

[12] N. Keshava and J. F. Mustard, "Spectral unmixing," *IEEE signal processing magazine*, vol. 19, no. 1, pp. 44–57, 2002.

[13] J. Hill and J. Mégier, *Imaging Spectrometry – a Tool for Environmental Observations*. Eurocourses: Remote Sensing, Springer Netherlands, 2007.

[14] B. Recht, M. Fazel, and P. A. Parrilo, "Guaranteed minimum-rank solutions of linear matrix equations via nuclear norm minimization," *SIAM review*, vol. 52, no. 3, pp. 471–501, 2010.

[15] P. Tseng and S. Yun, "A coordinate gradient descent method for nonsmooth separable minimization," *Mathematical Programming*, vol. 117, no. 1-2, pp. 387–423, 2009.

[16] P. Tseng, "Convergence of a block coordinate descent method for nondifferentiable minimization," *Journal of optimization theory and applications*, vol. 109, no. 3, pp. 475–494, 2001.

[17] F. Zhu, Y. Wang, B. Fan, S. Xiang, G. Meng, and C. Pan, "Spectral unmixing via data-guided sparsity," *IEEE Transactions on Image Processing*, vol. 23, no. 12, pp. 5412–5427, 2014.

[18] E. Vargas, H. Arguello, and J.-Y. Tourneret, "Spectral image fusion from compressive measurements using spectral unmixing," in *Proc. of 7th International Workshop on Computational Advances in Multi-Sensor Adaptive Processing (CAMSAP17)*, pp. 10–13, 2017.


ISBN 978-90-827970-1-5 © EURASIP 2018